Applications of Mathematics

Wenhuan Ai; Ting Zhang; Dawei Liu Bifurcation analysis of macroscopic traffic flow model based on the influence of road conditions

Applications of Mathematics, Vol. 68 (2023), No. 4, 499-534

Persistent URL: http://dml.cz/dmlcz/151707

Terms of use:

© Institute of Mathematics AS CR, 2023

Institute of Mathematics of the Czech Academy of Sciences provides access to digitized documents strictly for personal use. Each copy of any part of this document must contain these *Terms of use*.



This document has been digitized, optimized for electronic delivery and stamped with digital signature within the project $\mathit{DML-CZ}$: The Czech Digital Mathematics Library http://dml.cz

BIFURCATION ANALYSIS OF MACROSCOPIC TRAFFIC FLOW MODEL BASED ON THE INFLUENCE OF ROAD CONDITIONS

WENHUAN AI, TING ZHANG, DAWEI LIU, Lanzhou

Received July 19, 2022. Published online May 18, 2023.

Abstract. A macroscopic traffic flow model considering the effects of curves, ramps, and adverse weather is proposed, and nonlinear bifurcation theory is used to describe and predict nonlinear traffic phenomena on highways from the perspective of global stability of the traffic system. Firstly, the stability conditions of the model shock wave were investigated using the linear stability analysis method. Then, the long-wave mode at the coarse-grained scale is considered, and the model is analyzed using the reduced perturbation method to obtain the Korteweg-de Vries (KdV) equation of the model in the sub-stable region. In addition, the type of equilibrium points and their stability are discussed by using bifurcation analysis, and a theoretical derivation proves the existence of Hopf bifurcation and saddle-knot bifurcation in the model. Finally, the simulation density spatio-temporal and phase plane diagrams verify that the model can describe traffic phenomena such as traffic congestion and stop-and-go traffic in real traffic, providing a theoretical basis for the prevention of traffic congestion.

Keywords: macro traffic flow; curves; ramps; bifurcation analysis

MSC 2020: 35A35

1. Introduction

With the increasing number of vehicles in the city, various traffic problems have gradually emerged. Traffic congestion has become one of the main factors of traffic problems, which restricts the rapid development of cities. How to alleviate traffic problems with the guidance of scientific theories has become a hot topic of research

DOI: 10.21136/AM.2023.0163-22 499

This work is partially supported by the National Natural Science Foundation of China under Grant No. 61863032 and the Natural Science Foundation of Gansu Province of China under Grant No. 20JR5RA533 and the China Postdoctoral Science Foundation Funded Project (Project No.: 2018M633653XB) and the "Qizhi" Personnel Training Support Project of Lanzhou Institute of Technology (2018QZ-11) and Gansu Province Educational Research Project (Grant No. 2021A-166).

nowadays. Many experts and scholars have proposed many traffic flow models in order to study the formation and propagation characteristics of traffic congestion.

Classical traffic flow models can be divided into microscopic traffic flow models and macroscopic traffic flow models. The main microscopic models are the vehiclefollowing model [30], [31], [24], [25] and the metric automata model [5], [6]; the main macroscopic models are the continuous flow model [35], [9] and the lattice fluid dynamics model [34], [32], [33], [36]. In the study of traffic flow models, Gupta and Katiyar presented many important findings, and in 2005, they studied a new anisotropic continuous traffic flow model, analyzed some certain qualitative properties of the model, and discussed the relationship between shock waves in traffic flow and traffic congestion [10]. In 2006, they conducted a study based on a modified anisotropic continuum model and obtained the transitions between free flow and various types of congested flows through numerical simulations, observing several states such as local clustering and stop-and-go. The results show that the model is able to describe all three phases of the traffic flow developed by kerner [12]. In addition, they developed a new continuous model containing anisotropy term based on an improved car-following model. It was found that this anisotropic term ensures that the characteristic velocity is always less than or equal to the macroscopic flow velocity, and this new model also overcomes the problem of negative flow and negative velocity that exists in almost every higher-order continuous medium model [11]. In the study by Gupta and Sharma, they discussed a study of the nonlinear stability of a new anisotropic continuum traffic flow model in which the dimensionless parameter or anisotropic factor controls the nonisotropic character and diffusive influence [14]. Shock waves and sparse waves, local clustering effects, and phase transitions are investigated through experimental simulations of a two-lane continuous medium model with coupling effects and are found to be consistent with various nonlinear dynamical phenomena observed in real traffic flows. The results show that the model is able to explain some specific traffic phenomena and is consistent with the real traffic flow [15]. In the studies considering the effect of optimal current difference on traffic dynamics, many new lattice hydrodynamic models have been proposed to investigate the significant effect of optimal current difference on traffic dynamics, which is beneficial to curb traffic congestion [13]. Besides, based on the study of lattice hydrodynamic model, many scholars have done a lot of research considering the effects of different vehicle ratios, leading vehicle information, and delayed feedback on traffic congestion [28]. The microscopic model focuses on studying and analyzing the traffic operation of individual vehicles and is constructed based on the velocity, headway time distance and acceleration information of vehicles; while the macroscopic model studies the traffic operation of the road traffic flow as a whole, which can take into account the road conditions themselves, as well as the factors of traffic flow and other random disturbances that affect road traffic safety. The expression of the macroscopic model is based on the partial differential equation of density and velocity, which has higher computational efficiency in comparison. In this paper, we select the continuous model, which is a classical macroscopic traffic flow model.

In the real traffic environment, the vehicle driving will be affected by the road geometry and weather environment and other random interference factors. When the driver encounters a turn or goes up or down a ramp while driving, the blind spot of the sight area existing on the curve and the too steep ramp will affect the driving, which will lead to traffic chaos, thus increasing the chance of traffic congestion and traffic accidents. In addition, the impact of weather conditions on traffic flow cannot be ignored. When there is rain, snow, haze and other weather, visibility and ground adhesion will be reduced, which will lead to unstable vehicle velocity; while in good weather conditions, driving will hardly be affected. In 2014, Zeng et al. [29] studied the effect of road curves on single-lane traffic flow, and proposed a cellular model (CA) with road curves based on the NaSch model to examine the traffic flow under different conditions such as curve radius, arc length, and road friction coefficient by taking the curve characteristics as the study object. The simulation results showed that the smaller the radius of the curve, the more likely blockage occurs. In 2017, Meng et al. [26] proposed a new traffic flow model to describe the movement behavior of vehicles on curved roads with slopes. The relevant effects on uniform traffic congestion were investigated using analytical and numerical methods. Based on the control theory, the condition of no traffic congestion is obtained analytically. Finally, the developed traffic flow model is validated by simulation. Theoretical and numerical results show that the relevant factors such as friction coefficient, radius of curvature, curve slope and parameters have a large influence on the traffic flow stability. In 2020, Zhang et al. [37] studied a macroscopic traffic flow model that considered the velocity difference between adjacent vehicles on uphill and downhill, analyzed the stability of the model, simulated the spatial and temporal evolution of traffic flow on uphill and downhill, and concluded that the unstable region on downhill expands as the gradient increases. In 2022, Li et al. [22] analyzed the modeling law of a new continuous medium model considering the self-stability control of sidehill curves, and studied the potential influencing factors of vehicle steadystate velocity, historical velocity, road curve radius and road slope on the stability of traffic flow, based on which an extended continuous model considering the selfstability effect of sidehill curves was proposed, stability analysis was performed, and the simulation of different slope and radius under self-stabilization effect, which shows that the self-stabilization effect is beneficial to reduce congestion on curved roads with slopes.

Therefore, taking realistic factors into account in the traffic system is not only more consistent with the actual situation of the road and can improve the safety and stability of road traffic, but also more accurate, reliable and realistic for the study of traffic flow theory. In view of this fact, we improved a new macroscopic traffic flow model by considering the influence of factors such as curves, ramps and weather environment on traffic conditions.

In complex traffic systems, a variety of nonlinear traffic phenomena are often presented, and these nonlinear traffic phenomena are also subject to frequent alternating changes. Theoretically, the nature of such changes is a bifurcation behavior, and in order to study the impact of these changes on the stability of traffic flow, bifurcation theory was introduced into traffic flow to reproduce the sudden changes that occur in the traffic system. At present, the bifurcation phenomenon in traffic systems is mainly studied from the follow-along model, while the analysis of the bifurcation phenomenon in macroscopic traffic flow models is not very common. In 1999, Igarashi et al. and Orosz et al. investigated the bifurcation phenomenon of traffic flow in the Optimal Velocity model [17], [16], [27] proposed by Bando et al. Igarashi et al. proved the existence of Hopf bifurcation by a rigorous mathematical derivation. Orosz et al. determined the type of Hopf bifurcation by drawing a bifurcation simulation diagram and described its stability. In 2009, Ling et al. [23] studied the bifurcation phenomenon of traffic flow in a nonlinear follow-along model by applying the theory of time-lag dynamical systems, and analyzed the stability of the system consisting of three vehicles and its Hopf bifurcation. In 2013, Carrillo et al. [4] investigated the macroscopic second-order traffic flow model and proved the existence of the Taken-Bogdanov bifurcation. In 2015, Delgado et al. [8] applied traveling wave solution for traffic flow to prove the existence of the TB bifurcation, thus explaining the existence of the Hopf bifurcation and the GH bifurcation. In order to describe in detail the specific traffic flow phenomena caused by bifurcation, Ai et al. [1] derived the conditions for the existence of Hopf bifurcations of the velocity gradient macroscopic model, the types of Hopf bifurcations and their stability, and analyzed the traffic conditions near the bifurcation points by drawing simulation diagrams to explain the nonlinear traffic phenomena in complex ground transportation systems innovatively with bifurcation theory.

In order to study the bifurcation phenomenon in nonlinear traffic systems, the modified macroscopic traffic flow model mentioned above is analyzed using bifurcation analysis to investigate the nonlinear dynamics of traffic flow under bifurcation threshold and bifurcation conditions. By setting different parameters for the model, the type of equilibrium points and the stability of the traffic system under different conditions can be obtained. Theoretical analysis of the model can lead to the existence conditions and bifurcation types of Hopf bifurcation and Saddle-node bi-

furcation, and finally, the sudden changes of the stability of the traffic system near the Hopf bifurcation point and Saddle-node bifurcation point can be reproduced by a simulation diagram. By bifurcation analysis of the model, we can clearly explain how the qualitative state of this traffic flow system will change abruptly when the traffic parameters change and exceed a certain critical value, which will also reveal that bifurcation will lead to abrupt changes in the stability behavior of traffic flow. Thus, the bifurcation analysis theory of traffic flow provides a theoretical and scientific basis for preventing and alleviating traffic congestion, and explains the formation mechanism of traffic congestion.

The paper is structured as follows: Section 2 presents the improved model considering the effects of curved ramps and weather conditions on traffic flow; in Section 3, a linear stability analysis of the model is performed to derive the neutral stability condition of the model; Section 4 derives the KdV-Burger equation based on the nonlinear stability analysis; in Section 5, the model is analyzed using bifurcation theory to study nonlinear traffic phenomena in the transportation system; Section 6 validates and explains the theoretical analysis part by means of simulation plots; Section 7 concludes the full work.

2. Model introduction

In early traffic dynamics studies, many researchers neglected the effect of driver response phenomenon. To address this phenomenon, in 1995, Bando et al. [2] developed the well-known OV traffic flow model (OVM) by introducing an optimal velocity function. The OV model can describe many characteristics, such as the instability of traffic flow, the evolution of traffic congestion, and the stop-and-go phenomenon. The expression of the model is

(2.1)
$$\frac{\mathrm{d}v_n(t)}{\mathrm{d}t} = a[V(\Delta x_n(t)) - v_n(t)],$$

where a is the driver's sensitivity; $v_n(t)$ and $\Delta x_n(t)$ represent the instantaneous velocity and headway of vehicle n at moment t, respectively; $V(\Delta x_n(t))$ represents the optimal velocity function, which is defined as

(2.2)
$$\frac{V_{\text{max}}}{2} \{ \tanh[\Delta x_n(t) - h_c] + \tan(h_c) \},$$

where $V_{\rm max}$ and h_c are the maximum vehicle velocity and the allowable safety distance, respectively.

Considering the problems of excessive acceleration and impractical deceleration in the OV model, Jiang et al. [18] proposed the Full Velocity Difference (FVD) model in 2001, and the FVD model expression is as follows

(2.3)
$$\frac{\mathrm{d}v_n(t)}{\mathrm{d}t} = a[V(\Delta x_n(t)) - v_n(t)] + \lambda \Delta v_n(t).$$

The FVD model improves the unrealistic acceleration problem of the OV model and obtains the kink wave in the crowded condition by simulation. Therefore, the FVD model is more mature and has superior steady-state and dynamic performance compared with the previous follower model.

In the real traffic environment, the vehicle driving will be affected by road geometry and weather and other random interference factors. Relative to ordinary roads, curves and ramps on the driving interference, order chaos, stability is poor, the driver's risky driving behavior increased, it is easy to occur traffic congestion and traffic accidents. In addition, the vehicle driving velocity is relatively stable under good weather conditions; bad weather conditions will have an impact on the driver's sight distance and road adhesion, and the vehicle driving velocity is relatively unstable. In order to improve the safety of road traffic, it is necessary for drivers to consider the influence brought by curves and ramps in the process of driving. Therefore, taking realistic factors into account in the traffic system is not only more consistent with the actual situation of the road and can improve the safety and stability of road traffic, but also more accurate, reliable and practical for the study of traffic flow theory. The following is to analyze the impact of different real factors on traffic flow separately.

The curve shape refers to the curve, and its characteristic parameter is the radius of curvature. Therefore, the research on the influence of road curve on the following vehicle can start from the radius of curvature of the curve. Visually, the "distance" between the following vehicle and the vehicle in front becomes smaller when driving on a curved road. Therefore, when the following vehicle is stimulated, its response is different from that on a straight road. The response of the following vehicle to the guiding vehicle can be studied from two aspects.

For the vehicle in the curve road, different driving velocity required for the minimum safety radius of curvature is not the same—the higher the velocity, the greater the minimum safety radius of curvature; conversely, the lower the velocity, the minimum safety radius of curvature required will be smaller. Assuming that during driving in a curve, the guiding vehicle suddenly accelerates, but the driver of the following vehicle will have visual illusion due to being in the curve, which will cause him to intuitively feel that the "straight line distance" between himself and the guiding vehicle does not increase significantly, and mistakenly believe that the headway

between the two vehicles has hardly changed. Therefore, its response to guiding the vehicle to accelerate is relatively weak. Assume that r is the actual radius of curvature of a curved road section, and r_0 is the minimum safe radius of curvature required for a vehicle traveling on that curved road section at a certain velocity. The difference in acceleration resulting from the influence of a curve compared to a straight section is

(2.4)
$$a_{\Delta} = \xi \tanh\left(1 - \frac{r_0}{r}\right).$$

In (2.4), a_{Δ} represents the difference in acceleration resulting from following the vehicle driving in a curve versus driving in a straightaway when the guiding vehicle to accelerate, and ξ represents the influence coefficient. And r_0 can be calculated by feeding the following equation

$$(2.5) r_0 = \frac{v^2}{127\mu}.$$

When driving on a curved road section, if the guiding vehicle suddenly decelerates, that is, when $a_{n+1} < 0$, the driver of the following vehicle will have a certain visual illusion that the headway between the two vehicles suddenly decreases, and at this time, the driver's reaction is stronger relative to the reaction when driving on a straight road section, and the acceleration of the following vehicle will be greater at this time than that on a straight road section. Assume that r is the actual radius of curvature of a curved road section, and r_0 is the minimum safe radius of curvature required for a vehicle traveling on that curved road section at a certain velocity. The difference in acceleration resulting from the influence of a curve compared to a straight section is

(2.6)
$$a_{\Delta} = \xi \tanh\left(1 - \frac{r_0}{r}\right).$$

In the curve driving, regardless of whether the guiding vehicle is in an accelerating or decelerating state, the expression of the acceleration difference a_{Δ} generated by the following vehicle is the same. When the guiding vehicle to accelerate, the following vehicle also accelerates; when the guiding vehicle to decelerate, the following vehicle also decelerate.

Generally speaking, in order to ensure traffic safety, the driving velocity of the vehicle on the ramp will be smaller than that on the straight road. At this time, the following vehicle reacts strongly to the stimulation of the guiding vehicle, and the following vehicle always wants to maintain a larger headway with the guiding vehicle. When the vehicle goes uphill, the following vehicle is worried that the guiding

vehicle will suddenly decelerate (i.e., when $a_{n+1} < 0$), so the stimulus response to the guiding vehicle will be stronger than in the case of driving on the flat road, and the acceleration of the following vehicle will be greater than that on the flat road at this time; while the vehicle goes downhill, the following vehicle will not only worry about the guiding vehicle due to the faster driving velocity and sudden emergency braking (i.e., $a_{n+1} < 0$), but also worry that its own vehicle will occur brake failure, which will lead to the driver of the following vehicle reacts to the stimulus of the guiding vehicle significantly stronger than in the case of driving on a flat road, the following vehicle reacts to the stimulus of the guiding vehicle significantly stronger than in the case of driving on a flat road, and the acceleration of the following vehicle is still greater than that on a flat road [15]. Assuming that the vehicle is driving on a road section with slope, the acceleration difference generated by the following vehicle compared to the flat road can be expressed as

$$(2.7) a_{\Delta} = \xi \tanh(1-i).$$

In (2.7), a_{Δ} denotes the difference in acceleration generated by following the vehicle when the slope factor is considered, ξ denotes the influence coefficient, and the slope value i is in percentage form and is determined by the slope angle θ of the road section, which can be defined as

$$(2.8) i = \frac{\theta}{90^{\circ}}.$$

The impact of bad weather on vehicle driving is mainly manifested in the reduction of the driver's visual distance and the reduction of road adhesion. The variable φ represents the complexity of weather conditions, which mainly affects the driver's sight distance and road surface adhesion. The variables s_0 and φ are used to represent the driver's sight distance and road adhesion, respectively, while s_0 and φ are the values taken under ideal weather conditions. The expression is as follows:

$$\phi = \frac{s_0}{s} \cdot \frac{\varphi_0}{\varphi}.$$

It can be seen that in an ideal climate, the effect of environmental complexity is the lowest when $\phi = s_0 \varphi_0/(s\varphi) = 1$. However, in practice the values are generally greater than 1, and the effect of ϕ on acceleration is as follows:

(2.10)
$$a_{\Delta} = \xi \tanh\left(1 - \frac{s_0}{s} \cdot \frac{\varphi_0}{\varphi}\right).$$

In (2.10), a_{Δ} represents the acceleration difference generated by the following vehicle when considering the driver's sight distance s and road surface adhesion φ . When

the guiding vehicle accelerates, the following vehicle will also accelerate, the driver will appropriately reduce the response to the acceleration behavior of the preceding vehicle due to the influence of the sight distance and road surface adhesion, so the acceleration at this time will be less than the acceleration when driving in the ordinary roadway (i.e., $a_{\Delta} < 0$). When the lead vehicle decelerates, the following vehicle will also decelerate, but at this time, due to the reduced sight distance and road surface adhesion, the driver's reaction to the front vehicle's deceleration behavior is stronger, so the acceleration at this time will be greater than the acceleration when driving on the ordinary road (i.e., $a_{\Delta} > 0$). ξ indicates the influence coefficient.

Combining the acceleration differences generated in the three cases yields a general expression for the acceleration difference generated under the influence of multiple factors

(2.11)
$$a_{\Delta} = \xi \tanh\left(1 - \frac{r_0}{r} \cdot \frac{s_0}{s} \cdot \frac{\varphi_0}{\varphi} \cdot i\right).$$

Through the analysis of various traffic scenarios mentioned above, we have come to the conclusion that when driving on curves, ramps, and adverse weather conditions, if the guiding vehicle to accelerate, the acceleration of the following vehicle will be less than acceleration of driving on ordinary road sections. If the guiding vehicle to decelerate, the acceleration of the following vehicle will be greater than acceleration of driving on a ordinary road section. When guiding the vehicle to slow down, the response of the following vehicle to the deceleration of the vehicle in front of it is greater than the response in the normal roadway situation, so its acceleration will be greater than the usual acceleration. Therefore, a function $u_n(t)$ is used to control the influence of the above disturbance factors on the acceleration, given as

(2.12)
$$u_n(t) = \begin{cases} -1, & a_{n+1} > 0, \\ 1, & a_{n+1} < 0. \end{cases}$$

The function $u_n(t)$ is a binary variable that reflects whether the front vehicle is accelerating or decelerating.

In view of the above analysis, we introduce the effects of curves, ramps and weather conditions on traffic conditions into the FVD model to produce the new followership model

(2.13)
$$\frac{\mathrm{d}v_n(t)}{\mathrm{d}t} = a[V(\Delta x_n(t)) - v_n(t)] + \lambda \Delta v_n(t) + u_n(t)H_n(t),$$

where $H_n(t)$ is a small perturbation generated under the influence of curved ramps and weather conditions, which is defined as follows

(2.14)
$$H_n(t) = \xi \tanh\left(1 - \frac{r_0}{r} \cdot \frac{s_0}{s} \cdot \frac{\varphi_0}{\varphi} \cdot i\right) \times \Delta v_n(t).$$

In order to transform the above micro traffic flow model into a macro traffic flow model [19], the following variables are introduced

(2.15)
$$v_n(t) \to v(x,t), \quad v_{n+1}(t) \to v(x+\Delta,t),$$
$$V(\Delta x_n(t)) \to V_e(\varrho), \quad V'(\Delta x_n(t)) \to -\varrho^2 V'_e(\varrho),$$

where Δ represents the distance of continuous vehicles, $\varrho(x,t)$ and v(x,t) represent the macro density and macro velocity respectively, and $V_e(\varrho)$ is the equilibrium velocity.

By performing a Taylor expansion on the variable $v_{n+1}(t)$ and neglecting the higher order terms, we obtain

(2.16)
$$\Delta v_n(t) = v(x + \Delta, t) - v(x, t) = \Delta v_x + \frac{1}{2} \Delta^2 v_{xx}.$$

According to the above conversion, (2.13) can be rewritten as follows

$$(2.17) v_t + (v - \lambda \Delta - N\Delta)v_x = a[V_e(\varrho) - v] + \frac{1}{2}(\lambda + N)\Delta^2 v_{xx}.$$

For simplification, $\xi \tanh(1-r_0s_0\varphi_0i/(rs\varphi))$ will be replaced by N in the derivation that follows, as:

(2.18)
$$N = \xi \tanh\left(1 - \frac{r_0}{r} \cdot \frac{s_0}{s} \cdot \frac{\varphi_0}{\varphi} \cdot i\right).$$

Combining (2.17) with a local vehicle number conservation equation, the following new macro continuous traffic flow model equation is obtained:

(2.19)
$$\begin{cases} \varrho_t + \varrho v_x + v \varrho_x = 0, \\ v_t + \left(v - \lambda \Delta - \xi \tanh\left(1 - \frac{r_0}{r} \cdot \frac{s_0}{s} \cdot \frac{\varphi_0}{\varphi} \cdot i\right) \Delta\right) v_x \\ = a[V_e(\varrho) - v] + \frac{1}{2} \left(\lambda + \xi \tanh\left(1 - \frac{r_0}{r} \cdot \frac{s_0}{s} \cdot \frac{\varphi_0}{\varphi} \cdot i\right)\right) \Delta^2 v_{xx}. \end{cases}$$

3. Linear stability analysis

Rewrite (2.19) in the following vector form to facilitate subsequent analysis

$$(3.1) U_t + AU_x = E,$$

where

(3.2)
$$U = \begin{bmatrix} \varrho \\ v \end{bmatrix}, \quad \mathbf{A} = \begin{bmatrix} v & \varrho \\ 0 & v - \lambda \Delta - N \Delta \end{bmatrix},$$

(3.3)
$$E = \begin{bmatrix} 0 \\ a[V_e(\varrho) - v] + \frac{1}{2}(\lambda + N)\Delta^2 v_{xx} \end{bmatrix}.$$

By solving the equation, the eigenvalue of A can be obtained as:

(3.4)
$$\lambda_1 = v, \quad \lambda_2 = v - \lambda \Delta - N\Delta.$$

The above characteristic velocities $\lambda_{(i=1,2)}$ are not greater than the macroscopic traffic flow velocity, which proves that the model is anisotropic. Therefore, the model describes traffic phenomenon in which the vehicles behind do not affect the movement of the vehicles in front.

Regarding the model, it has limitations with respect to certain parameters. r is the actual radius of curvature of a road section, while r_0 is the minimum safe radius of curvature required at a given velocity, so that the value of r must be greater than the value of r_0 in order to ensure safe driving, that is $r \ge r_0$. The expression for the weather complexity is $\phi = s_0 \varphi_0/(s\varphi)$. The lowest value that can be obtained under ideal weather conditions, at this point, $\phi = 1$; when the weather conditions are not ideal, the value of ϕ is greater than 1, that is, $\phi > 1$. Based on a comprehensive analysis of the two scenarios, it can be concluded that the value of weather complexity ϕ is greater than or equal to 1. The above discussion of the range of values for the parameters is to ensure model rationality.

In addition to the limitations of the parameters mentioned above, the factors considered in the model developed in this paper are not comprehensive enough, which leads to limitations in the scope of application of the model. In fact, the model is suitable for describing traffic flow under specific conditions such as curves, ramps and bad weather. In addition, the model is a macroscopic traffic flow model and has limitations of its own. It is an effective tool for simulating mass traffic and is suitable for simulating highway traffic flows, but not street traffic. Finally, the model is also unable to describe the overtaking or lane changing behaviour of vehicles on a single lane.

We take the density and velocity of the initial traffic flow as constants ϱ_0 and v_0 , and then add a small perturbation to the density and velocity of the initial traffic flow. The small perturbation takes the form

(3.5)
$$\begin{pmatrix} \varrho(x,t) \\ v(x,t) \end{pmatrix} = \begin{pmatrix} \varrho_0 \\ v_0 \end{pmatrix} + \begin{pmatrix} \widehat{\varrho}_k \\ \widehat{v}_k \end{pmatrix} \exp(ikx + \sigma_k t),$$

where k and σ_k denote wave number and frequency, respectively.

By substituting (3.5) into (2.19), we can obtain the following equation

$$(3.6) \qquad \begin{cases} (\sigma_k + v_0 ik)\widehat{\varrho}_k + \varrho_0 ik\widehat{v}_k = 0, \\ aV'_e(\varrho_0)\widehat{\varrho}_k - [\sigma_k + (v_0 - \lambda\Delta - N\Delta)ik + a - \frac{1}{2}(\lambda + N)\Delta^2(ik)^2]\widehat{v}_k = 0. \end{cases}$$

If there exists a nonzero solution to (3.6), then the determinant of its coefficients must be equal to zero, i.e.

(3.7)
$$\begin{vmatrix} \sigma_k + v_0 ik & \varrho_0 ik \\ aV'_e(\varrho_0) & -[\sigma_k + (v_0 - \lambda \Delta - N\Delta)ik + a - \frac{1}{2}(\lambda + N)\Delta^2(ik)^2] \end{vmatrix} = 0,$$

therefore

$$(3.8) (\sigma_k + v_0 ik)^2 + aV'_e(\varrho_0)\varrho_0 ik + (\sigma_k + v_0 ik)[a - (\lambda + N)\Delta ik - \frac{1}{2}(\lambda + N)\Delta^2(ik)^2] = 0.$$

To determine the value of σ_k , we perform a power series expansion of σ_k , i.e., $\sigma_k = \sigma_1 i k + \sigma_2 (i k)^2 + \ldots$, and combine the terms into (3.8) to obtain a second-order expression for i k as

$$(3.9) \left[aV_e'(\varrho_0)\varrho_0 + (\sigma_1 + v_0)a \right] ik + \left[(\sigma_1 + v_0)^2 + \sigma_2 a - (\sigma_1 + v_0)(\lambda + N)\Delta \right] (ik)^2 = 0.$$

In order to ensure that the above equation holds, the first-order term ik and the second-order term $(ik)^2$ of the power series must be equal to zero. Thus, the following equation can be obtained

(3.10)
$$aV'_{e}(\varrho_{0})\varrho_{0} + (\sigma_{1} + v_{0})a = 0,$$

(3.11)
$$(\sigma_1 + v_0)^2 + \sigma_2 a - (\sigma_1 + v_0)(\lambda + N)\Delta = 0.$$

Combining (3.10) and (3.11) and then solving them, we can derive the equation

(3.12)
$$\sigma_1 = -v_0 - V_e'(\varrho_0)\varrho_0,$$

(3.13)
$$\sigma_2 = -\frac{V_e'(\varrho_0)\varrho_0}{a} [V_e'(\varrho_0)\varrho_0 + (\lambda + N)\Delta].$$

When $\sigma_2 > 0$, the traffic flow is stable, so the neutral stability condition satisfies the following equation:

$$(3.14) a_s = V_e'(\rho_0)\rho_0[V_e'(\rho_0)\rho + (\lambda + N)\Delta].$$

By using Taylor expansion, (3.6) is rewritten as

(3.15)
$$\operatorname{Im}(\sigma_k) = -k[v_0 + \varrho_0 V_e'(\varrho_0)] + O(k^3).$$

According to (3.15), the following can be obtained:

$$(3.16) c(\varrho_0) = v_0 + \varrho_0 V_e'(\varrho_0).$$

4. Nonlinear stability analysis

In order to analyze the evolutionary behavior of small perturbations near neutral stability conditions of the traffic system, a new coordinate system is introduced to translate it into the form

$$(4.1) z = x - ct.$$

Substituting the above equation into (2.19) yields

(4.2)
$$\begin{cases} -c\varrho_z + q_z = 0, \\ -cv_z + (v - \lambda\Delta - N\Delta)v_z = a[Ve(\varrho) - v] + \frac{1}{2}(\lambda + N)\Delta^2 v_{zz}, \end{cases}$$

where the traffic flow q is the product of density and velocity, i.e., $q = \varrho v$, which can be obtained by substituting the flow equation into (4.2)

$$v_z = \frac{c\varrho_z}{\varrho} - \frac{q\varrho_z}{\varrho^2},$$

$$v_{zz} = \left(\frac{c}{\varrho} - \frac{q}{\varrho^2}\right)\varrho_{zz} - 2\left(\frac{c}{\varrho^2} - \frac{q}{\varrho^3}\right)\varrho_z^2.$$

A second-order Taylor expansion for the flow rate q yields

$$(4.5) q = \varrho V e(\varrho_0) + b_1 \varrho_z + b_2 \varrho_{zz}.$$

Substituting (4.3)–(4.4) into the second equation of (4.2) yields

$$(4.6) -c\left(\frac{c\varrho_z}{\varrho} - \frac{q\varrho_z}{\varrho^2}\right) + \left(\frac{q}{\varrho} - \lambda\Delta - N\Delta\right)\left(\frac{c\varrho_z}{\varrho} - \frac{q\varrho_z}{\varrho^2}\right)$$

$$= a\left[V_e(\varrho) - \frac{q}{\varrho}\right] + \frac{1}{2}(\lambda + N)\Delta^2\left(\frac{c\varrho_{zz}}{\varrho} - \frac{2c\varrho_z^2}{\varrho^2} - \frac{q\varrho_{zz}}{\varrho^2} + \frac{2q\varrho_z^2}{\varrho^3}\right).$$

Since neither ϱ_z nor ϱ_{zz} is zero, the coefficients of ϱ_z and ϱ_{zz} in (4.6) must be zero, so we can get

(4.7)
$$\begin{cases} b_1 = \frac{1}{a} [(c - V_e(\varrho))(c + (\lambda + N)\Delta^2) - cV_e(\varrho)], \\ b_2 = \frac{1}{2a} (\lambda + N)\Delta^2 [c - V_e(\varrho)]. \end{cases}$$

Near the neutral stability condition, taking $\varrho = \varrho_h + \widehat{\varrho}(x,t)$, a second-order Taylor expansion for ϱ yields

$$(4.8) \varrho V_e(\varrho) \approx \varrho_h V_e(\varrho_h) + (\varrho V_e)_{\varrho} \big|_{\varrho = \varrho_h} \widehat{\varrho} + \frac{1}{2} (\varrho V_e)_{\varrho\varrho} \big|_{\varrho = \varrho_h} \widehat{\varrho}^2.$$

Substituting the above equation into $q = \varrho V e(\varrho_0) + b_1 \varrho_z + b_2 \varrho_{zz}$ and combining with (4.6), we can obtain

$$(4.9) -c\varrho_z + [(\varrho V_e(\varrho))_{\varrho} + (\varrho V_e(\varrho))_{\varrho\varrho} \varrho]\varrho_z + b_1\varrho_{zz} + b_2\varrho_{zzz} = 0.$$

In order to convert (4.9) to the standard KdV-Burgers equation, the following transformations need to be introduced

$$(4.10) U = -[(\varrho V_e)_{\varrho} + (\varrho V_e)_{\varrho\varrho}\varrho], \quad X = mx, \quad T = -mt.$$

Then, the following standard KdV-Burgers equation can be obtained by substituting (4.10) into (4.9)

$$(4.11) U_T + UU_X - mb_1U_{XX} - m^2b_2U_{XXX} = 0.$$

The following solutions are obtained by solving the above equations

$$(4.12) U = -\frac{3(-mb_1)^2}{25(-m^2b_2)} \left[1 + 2\tanh\left(\pm\frac{-mb_1}{10m^2}\right)\left(X + \frac{6(-mb_1)^2}{25(-m^2b_2)}T + \varsigma_0\right) + \tanh^2\left(\pm\frac{-mb_1}{10m^2}\right)\left(X + \frac{6(-mb_1)^2}{25(-m^2b_2)}T + \varsigma_0\right) \right].$$

5. Bifurcation analysis of mode

5.1. Types of equilibrium points and their stability. In this paper, we assume that the main section is open boundary condition, i.e.

(5.1)
$$\varrho(1,t) = \varrho(2,t), \ \varrho(L,t) = \varrho(L-1,t), \ v(1,t) = v(2,t), \ v(L,t) = v(L-1,t).$$

Assume that the model has traveling wave solutions $\varrho(z)$ and v(z), where z=x-ct and traveling wave velocity c<0. Based on the theory above, substituting into (2.19) yields

$$(5.2) -c\varrho_z + q_z = 0,$$

$$(5.3) -cv_z + (v - \lambda \Delta - N\Delta)v_z = a[Ve(\varrho) - v] + \frac{1}{2}(\lambda + N)\Delta^2 v_{zz}.$$

From (5.2) and (5.3)

$$(5.4) v_z = \frac{c\varrho_z}{\varrho} - \frac{q\varrho_z}{\varrho^2},$$

$$(5.5) v_{zz} = \left(\frac{c}{\rho} - \frac{q}{\rho^2}\right)\varrho_{zz} - 2\left(\frac{c}{\rho^2} - \frac{q}{\rho^3}\right)\varrho_z^2.$$

Substituting (5.4)–(5.5) into (5.3) yields

$$(5.6) -\frac{\varrho_z}{\varrho^3}q^2 + \left[\frac{(2c+\lambda\Delta+N\Delta)\varrho_z}{\varrho^2} + \frac{a}{\varrho} + \frac{(\lambda+N)\Delta^2\varrho_{zz}}{2\varrho^2}\right]q$$
$$= aV_{\varepsilon}(\varrho) + \frac{c^2 + c(\lambda\Delta+N\Delta)}{\varrho}\varrho_z + \frac{c(\lambda+N)\Delta^2}{2\varrho}\varrho_{zz}.$$

The integral of (5.2) gives

$$(5.7) -c\rho + q = \text{const.} = q^*,$$

that is,

$$(5.8) q = q^* + c\varrho.$$

Substituting (5.8) into (5.6) yields

$$(5.9) \left[\frac{(\lambda + N)\Delta^{2}(q^{*} + c\varrho)}{2\varrho} - \frac{c}{2}(\lambda + N)\Delta^{2} \right] \varrho_{zz}$$

$$- \left[\frac{(q^{*} + c\varrho)^{2}}{\varrho^{2}} - \frac{(2c + \lambda\Delta + N\Delta)(q^{*} + c\varrho)}{\varrho} + (c^{2} + c(\lambda\Delta + N\Delta)) \right] \varrho_{z}$$

$$+ a(q^{*} + c\varrho) - aV_{e}(\varrho) = 0.$$

The second-order ordinary differential equation for $\varrho(z)$ is obtained by simplification

(5.10)
$$\varrho_{zz} - G(\varrho, q^*)\varrho_z - F(\varrho, c, q^*) = 0,$$

where

(5.11)
$$G(\varrho, q^*) = \frac{2}{(\lambda + N)\Delta^2} \left[\frac{q^*}{\varrho} - \lambda \Delta - N\Delta \right],$$

(5.12)
$$F(\varrho, c, q^*) = -\frac{2\varrho}{T(\lambda + N)\Delta^2 q^*} [q^* + c\varrho - \varrho V_e(\varrho)].$$

Let $y = \frac{d\varrho}{dz}$, (5.4) can be transformed into a system of first-order ordinary differential equations

(5.13)
$$\begin{cases} \frac{\mathrm{d}\varrho}{\mathrm{d}z} = y, \\ \frac{\mathrm{d}y}{\mathrm{d}z} = G(\varrho, q^*)y + F(\varrho, c, q^*). \end{cases}$$

When making the right end of the system of (5.13) zero, it is possible to derive y = 0 and F = 0, from which its equilibrium point can be determined as $(\varrho_i, 0)$. A Taylor expansion of (5.13) at the equilibrium point gives the following linear system

(5.14)
$$\begin{cases} \varrho' = y, \\ y' = G(\varrho_i, q^*)y + F'(\varrho_i, c, q^*)(\varrho - \varrho_i). \end{cases}$$

The Jacobian matrix of system (5.13) at the equilibrium point $(\varrho_i, 0)$ can be derived as

$$(5.15) L = \begin{bmatrix} 0 & 1 \\ F_i' & G_i \end{bmatrix},$$

so, the Jacobian characteristic equation can be obtained as

$$\lambda^2 - G_i \lambda - F_i' = 0.$$

When $G_i = G(\varrho_i, q^*)$ and $F'_i = F'(\varrho_i, c, q^*)$, the following equations can be obtained from (5.11) and (5.12)

(5.17)
$$F_i' = -\frac{2\varrho_i}{T(\lambda + N)\Delta^2 q^*} [c - \varrho_i V_e'(\varrho_i) - V_e(\varrho_i)],$$

(5.18)
$$G_i = \frac{2}{(\lambda + N)\Delta^2} \left[\frac{q^*}{\varrho_i} - \lambda \Delta - N\Delta \right].$$

Since F = 0 at the equilibrium point, it follows that $q^* + c\varrho_i - \varrho_i V_e(\varrho_i) = 0$, so F_i' can be written as

(5.19)
$$F'_{i} = \frac{2(q^* + \varrho_{i}^{2}V_{e}(\varrho_{i}))}{T(\lambda + N)\Delta^{2}q^*}.$$

The type of equilibrium point of the system can be determined according to the qualitative theory of differential equations: (a) When $F_i'>0$, the equilibrium point is the saddle point; (b) When $G_i^2+4F_i'>0$ and $F_i'<0$, the equilibrium point is the node; (c) When $G_i^2+4F_i'<0$ and $G_i\neq 0$, the equilibrium point is the focus; (d) When $F_i'<0$ and $G_i=0$, the equilibrium point is the center. When $z\to\pm\infty$, the linear system is unstable at the saddle point; When $G_i<0$ (or $G_i>0$), it is stable at the node or focus with $z\to\infty$ (or $z\to-\infty$).

From the Hartman-Gorban linearization theorem we know that the nonlinear system (5.13) has the same equilibrium point as the linear system. For equilibrium points that are not central, the stability situation at the equilibrium point is the same for the nonlinear system (5.13) and the linear system (5.14). The equilibrium point ϱ_i (i = 1, 2, 3) of the linear system (5.8) can be solved when given any set of values of the traveling wave velocity and the traveling wave parameter q^* . The equilibrium velocity function proposed in the literature [20] is chosen:

(5.20)
$$V_e(\varrho) = V_f \left\{ \left[1 + \exp\left(\frac{\varrho/\varrho m - 0.25}{0.06}\right) \right]^{-1} - 3.72 \times 10^{-6} \right\},\,$$

where v_f is the free flow velocity and ϱ_m is the maximum or congestion density.

The values of parameters in this model are as follows (5.21)

$$T = 10 \,\mathrm{s}, \ V_f = 30 \,\mathrm{m/s}, \ \rho_m = 0.2 \,\mathrm{veh/m}, \ r_0 = 126 \,\mathrm{m}, \ r = 250 \,\mathrm{m}, \ \varphi = 4, \ i = 0.15.$$

When $\varrho = 0$, this is a mundane equilibrium point with no practical significance, so only other equilibrium points need to be discussed. From the discussion above and (5.17)–(5.18), the type of equilibrium point and its stability can be judged as shown in Table 1, where the equilibrium point is denoted by ϱ (i = 1, 2, 3).

Figure 1 (a) corresponds to the first set of data in Table 1. As seen in Figure 1 (a): When $z \to \pm \infty$, the system is unstable at the equilibrium points $(\varrho_1, 0)$ and $(\varrho_3, 0)$, and the trajectories in their vicinity are all far from this point. When $z \to \infty$, there are several spiral trajectories close to the saddle point $(\varrho_3, 0)$ converging to the focal point $(\varrho_2, 0)$; when $z \to -\infty$, these trajectories move away from this focal point and eventually converge to infinity. This shows that when $z \to \infty$, the system is stable at $(\varrho_2, 0)$; when $z \to -\infty$, the system is unstable at $(\varrho_2, 0)$, and the trajectory can be regarded as the saddle point-focus-saddle point solution of the system.

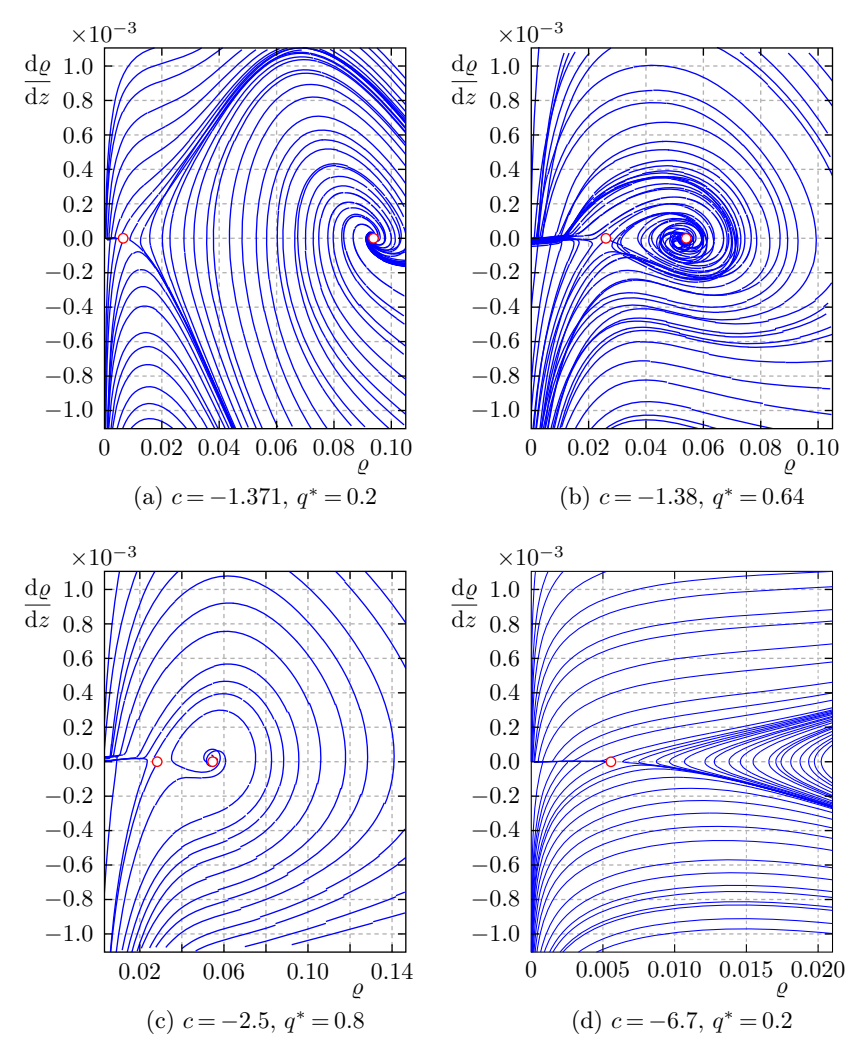


Figure 1. Phase plane diagram when the traveling wave velocity c and traveling wave parameter q^* take different values.

Figure 1 (b) corresponds to the second set of data in Table 1. Figure 1 (b) shows that when $z \to \pm \infty$, the system is unstable at the equilibrium point $(\varrho_1, 0)$, and its nearby trajectories are far away from this point. The spiral trajectory from (0.05, 0) tends to the focal point $(\varrho_2, 0)$ when $z \to \infty$, and the system is stable at that point; when $z \to -\infty$, it is far from the focal point $(\varrho_2, 0)$, and the system is unstable at that point. Further study reveals that the spiral trajectory from (0.03, 0) tends to the outermost circle of the curve ring in the figure when $z \to -\infty$ and tends to infinity when $z \to \infty$. Therefore, the system has a limit ring.

Figure 1 (c) corresponds to the third set of data in Table 1. Figure 1 (c) shows that when $z \to \pm \infty$, the system is unstable at the equilibrium point $(\varrho_1, 0)$, and all of its nearby tracks are far from this point. When $z \to -\infty$, the spiral trajectories close to the saddle point $(\varrho_1, 0)$ tend to the focal point $(\varrho_2, 0)$; when $z \to \infty$, these trajectories are far from the focal point and eventually tend to infinity. It follows that the system is stable at $(\varrho_2, 0)$ when $z \to -\infty$ and unstable at $(\varrho_2, 0)$ when $z \to \infty$.

Figure 1 (d) corresponds to the fourth set of data in Table 1. When $z \to \pm \infty$, the system is unstable at $(\varrho_1,0)$, and all the tracks in its vicinity move away from this point, and the value of the variable ϱ eventually tends to infinity. This indicates that the vehicle density corresponding to this set of parameters will continue to increase, the traffic system becomes unstable, and the traffic flow will eventually become congested.

(c,q)	ϱ_1	ϱ_2	ϱ_3		
	0.0065	0.0937	0.1447		
(-1.371, 0.2)	$F_i' > 0$, saddle point,	$\Delta_i < 0, G_i < 0$, focal point,	$F_i' > 0$, saddle point,		
	unstable for $z \to \pm \infty$.	stable for $z \to \infty$,	unstable for $z \to \pm \infty$.		
		unstable for $z \to -\infty$.			
	0.0254	0.0522			
(-1.38, 0.64)	$F_i' > 0$, saddle point,	$\Delta_i < 0, G_i < 0$, focal point,			
	unstable for $z \to \pm \infty$.	stable for $z \to \infty$,			
		unstable for $z \to -\infty$.			
	0.0283	0.0546			
(-2.5, 0.8)	$F_i' > 0$, saddle point,	$\Delta_i < 0, G_i < 0$, focal point,			
	unstable for $z \to \pm \infty$.	stable for $z \to \infty$,			
		unstable for $z \to -\infty$.			
	0.0065				
(-6.7, 0.2)	$F_i' > 0$, saddle point,				
	unstable for $z \to \pm \infty$.				

Table 1. Type of equilibrium point and its stability when model parameters are given, $\Delta_i - G_i^2 + 4F_i', i = 1, 2, 3.$

5.2. Derivation of Hopf bifurcation condition of model. The condition for the existence of the Hopf bifurcation is known from Lemma I [3].

Theorem 5.1. Consider the variable parameters of $x' = f(x, \lambda)$, $x \in R^n$, $\lambda \in R$, λ in the system. If (x_0, λ) satisfies the condition $f(x, \lambda)|_{(x_0, \lambda_0)} = 0_{n \times 1}$ of the equilibrium point, then there is $L = D_x f(x, \lambda)|_{(x_0, \lambda_0)}$, and its eigenvalue is $R(\varphi) \pm jI(\varphi)$. If $R(\varphi_0) = 0$ and $J(\varphi_0) = J_0 > 0$, $c = R'(\varphi)|_{\varphi_0} \neq 0$, then the system has Hopf bifurcations at $\varphi = \varphi_0$.

For system (5.13), let q^* be a variable parameter which has equilibrium point $(\varrho_0, 0)$ for all q^* . The derivative matrix at the equilibrium point is also the Jacobian matrix of the system at the equilibrium point, as follows: (5.22)

$$L(q^*) = \begin{pmatrix} 0 & 1 \\ \frac{2(q^* + \varrho^2 V_e'(\varrho))}{T(\lambda + N)\Delta^2 q^*} & \frac{2}{(\lambda + N)\Delta^2} \left(\frac{q^*}{\varrho} - (\lambda + N)\Delta\right) \end{pmatrix} \Big|_{\substack{\varrho = \varrho_0 \\ q^* = q_0^*}} \triangleq \begin{pmatrix} b_1 & b_2 \\ b_3 & b_4 \end{pmatrix}.$$

Let its eigenvalue be λ , and $\lambda = R(q^*) \pm jI(q^*)$, then its characteristic equation is as follows

(5.23)
$$\lambda^2 - (b_1 + b_4)\lambda + (b_1b_4 - b_2b_3) = 0.$$

Let the pair of eigenvalues of this equation be $R(q^*) \pm jI(q^*)$, then we can obtain

(5.24)
$$R(q^*) = \frac{b_1 + b_4}{2} = \frac{q * -(\lambda + N)\Delta \varrho_0}{(\lambda + N)\Delta^2 \varrho_0},$$

(5.25)
$$I(q^*) = \sqrt{(b_1b_4 - b_2b_3) - \frac{(b_1 + b_4)^2}{4}}$$
$$= \sqrt{\frac{-2q^* - 2\varrho^2 V_e'(\varrho)}{T(\lambda + N)\Delta^2 q^*} - \frac{(q^* - (\lambda + N)\Delta\varrho)^2}{[(\lambda + N)\Delta^2]\varrho^2}},$$

(5.26)
$$c = R'(q^*)|_{q^*0} = \frac{1}{(\lambda + N)\Delta^2 \varrho_0} \neq 0.$$

Let $R(\varrho_0, q_0^*) = 0$, then

(5.27)
$$R(\varrho_0, q_0^*) = \left(\frac{q_0^* - (\lambda + N)\Delta\varrho_0}{(\lambda + N)\Delta^2\varrho_0}\right)\Big|_{q^* = q_0^*} \triangleq 0,$$

therefore

$$q_0^* = (\lambda + N)\Delta\varrho_0.$$

At the same time,

(5.29)
$$I(\varrho_0, q_0^*) = \sqrt{\frac{-2q^* - 2\varrho^2 V_e'(\varrho)}{T(\lambda + N)\Delta^2 q^*} - \frac{(q^* - (\lambda + N)\Delta\varrho)^2}{[(\lambda + N)\Delta^2]\varrho^2}} \Big|_{\substack{\varrho = \varrho_0 \\ q^* = q_0^*}}$$

From (5.28)

(5.30)
$$I(\varrho_0, q_0^*) = \sqrt{\frac{-2q^* - 2\varrho^2 V_e'(\varrho)}{T(\lambda + N)\Delta^2 q^*}} \Big|_{\substack{\varrho = \varrho_0 \\ q^* = q_0^*}}.$$

Since $V'_e(\varrho) < 0$, it follows that $I(\varrho_0, q_0^*) > 0$ when $-\varrho_0^2 V_e(\varrho_0) > q_0^* > 0$. At this point the system has a Hopf bifurcation at $q^* = q_0^*$.

5.3. Derivation of Hopf bifurcation type of model. The principle of determining the Hopf bifurcation type can be known from Lemma II [3], [21].

Theorem 5.2. For system (5.13), there is a variable parameter q^* , which has a balance point $(\varrho_0, 0)$ for all q^* , let $\tilde{\varrho} = \varrho - \varrho_0$ translate the coordinates and move the balance point to the origin. At this time, the system can be expressed as follows

(5.31)
$$\begin{cases} \tilde{\varrho}' = y, \\ y' = \frac{2}{(\lambda + N)\Delta^2} \left(\frac{q^*}{\tilde{\varrho} + \varrho_0} - (\lambda + N)\Delta\right) y \\ -\frac{2(\tilde{\varrho} + \varrho_0)}{T(\lambda + N)\Delta^2 q^*} [q^* + c(\tilde{\varrho} + \varrho_0) - (\tilde{\varrho} + \varrho_0)V_e(\tilde{\varrho} + \varrho_0)]. \end{cases}$$

The linear form of Taylor expansion of the system at the equilibrium point $(\tilde{\varrho}, y) = (0, 0)$ is

$$\widetilde{x}' = L(q^*)\widetilde{x} + f,$$

wherein the constituent elements $f_{1,2}$ of the smooth vector function are Taylor expansions of the least quadratic term of \tilde{x} , which can be expressed as follows

(5.33)
$$f = \begin{bmatrix} 0 \\ k_{11}\tilde{\varrho}^2 + k_{22}y^2 + k_{12}\tilde{\varrho}y + k_{111}\tilde{\varrho}^3 + k_{222}y^3 + k_{112}\tilde{\varrho}^2y + k_{122}\tilde{\varrho}y^2 + o(\tilde{\varrho}, y)^4 \end{bmatrix}.$$

The form of Jacobian matrix $L(q^*)$ is

(5.34)

$$L(q^*) = \begin{pmatrix} 0 & 1 \\ \frac{2(q^* + \varrho_0^2 V_e'(\varrho_0))}{T(\lambda + N)\Delta^2 q^*} & \frac{2}{(\lambda + N)\Delta^2} \left(\frac{q^*}{\varrho_0} - (\lambda + N)\Delta\right) \end{pmatrix} = \begin{pmatrix} 0 & 1 \\ m(q^*) & n(q^*) \end{pmatrix},$$

its characteristic equations and eigenvalues are

where $\sigma = \sigma(q^*) = n(q^*) = \operatorname{tr} L(q^*), \ \Delta = \Delta(q^*) = -m(q^*) = \det L(q^*),$

(5.36)
$$\lambda_{12}(q^*) = \frac{1}{2}(\sigma(q^*) \pm \sqrt{\sigma(q^*)^2 - 4\Delta(q^*)}).$$

From Hopf bifurcation condition

(5.37)
$$\sigma(0) = 0, \quad \Delta(0) = I_0^2 > 0.$$

Introducing variables for smaller $|q^*|$,

(5.38)
$$R(q^*) = \frac{1}{2}\sigma(q^*), \quad I(q^*) = \frac{1}{2}\sqrt{4\Delta - \sigma^2(q^*)},$$

we can get its eigenvalue expression

(5.39)
$$\lambda_1(q^*) = \lambda(q^*), \quad \lambda_2(q^*) = \bar{\lambda}(q^*),$$

where

(5.40)
$$\lambda(q^*) = R(q^*) + jIq^*, \quad R(0) = 0, \quad I(0) = I_0 > 0.$$

Let the eigenvector of $L(q^*)$ corresponding to the eigenvalue $\lambda(q^*)$ be $I_{\rm re} + {\rm j}I_{\rm im}$, then

(5.41)
$$L(I_{\rm re} + jI_{\rm im}) = jI_0(I_{\rm re} + jI_{\rm im}).$$

Since the real and imaginary parts on both sides of the equation are equal, we get

(5.42)
$$\begin{cases} LI_{\text{im}} = I_0I_{\text{re}}, \\ LI_{\text{re}} = -I_0I_{\text{im}}. \end{cases}$$

Collating (5.42) yields the following relationship

(5.43)
$$L[I_{\text{im}} \quad I_{\text{re}}] = \begin{bmatrix} I_{\text{im}} \quad I_{\text{re}} \end{bmatrix} \begin{bmatrix} 0 & -I_0 \\ I_0 & 0 \end{bmatrix}.$$

It can be concluded that

$$[I_{\rm im} \quad I_{\rm re}]^{-1} L[I_{\rm im} \quad I_{\rm re}] = \begin{bmatrix} 0 & -I_0 \\ I_0 & 0 \end{bmatrix}.$$

Let

(5.45)
$$\widetilde{y} = \begin{bmatrix} I_{\text{im}} & I_{\text{re}} \end{bmatrix}^{-1} \widetilde{x}.$$

Then

(5.46)
$$\widetilde{y}' = \begin{bmatrix} I_{\rm im} & I_{\rm re} \end{bmatrix}^{-1} \widetilde{x}'.$$

520

Substituting (5.32) into (5.46) yields

(5.47)
$$\widetilde{y}' = \begin{bmatrix} I_{\text{im}} & I_{\text{re}} \end{bmatrix}^{-1} L \begin{bmatrix} I_{\text{im}} & I_{\text{re}} \end{bmatrix} \widetilde{y} + \begin{bmatrix} I_{\text{im}} & I_{\text{re}} \end{bmatrix}^{-1} f$$
$$= \begin{bmatrix} 0 & -I_{0} \\ I_{0} & 0 \end{bmatrix} \widetilde{y} + \begin{bmatrix} I_{\text{im}} & I_{\text{re}} \end{bmatrix}^{-1} f$$

and the eigenvector of $L(q^*)$ can be calculated as

(5.48)
$$I_{\text{re}} + jI_{\text{im}} = \begin{bmatrix} 0 \\ 1 \end{bmatrix} + j \begin{bmatrix} -\frac{1}{\sqrt{-m(q^*)}} \\ 0 \end{bmatrix}.$$

Substituting (5.29) and the values of $I_{\rm im}$ and $I_{\rm re}$ into (5.47) yields

$$\widetilde{y}' = \begin{bmatrix} 0 & -I_0 \\ I_0 & 0 \end{bmatrix} \widetilde{y}
+ \begin{bmatrix} 0 \\ k_{11}\widetilde{\rho}^2 + k_{22}y^2 + k_{12}\widetilde{\rho}y + k_{111}\widetilde{\rho}^3 + k_{222}y^3 + k_{112}\widetilde{\rho}^2y + k_{122}\widetilde{\rho}y^2 + O(\varrho, y)^4 \end{bmatrix}.$$

According to Lemma II, the value of a in system (5.13) can be calculated as

$$(5.50) a = (1/16)[\tilde{f}_{2\tilde{y}_1\tilde{y}_1\tilde{y}_2} + \tilde{f}_{2\tilde{y}_2\tilde{y}_2\tilde{y}_2}] + (1/16I_0)[-\tilde{f}_{2\tilde{y}_1\tilde{y}_2}(\tilde{f}_{2\tilde{y}_1\tilde{y}_1} + \tilde{f}_{2\tilde{y}_2\tilde{y}_2})].$$

Therefore, the value of c can be calculated as

(5.51)
$$c = R'(0) = \frac{1}{(\lambda + N)\Delta^2 \varrho_0} > 0.$$

Based on the above analysis, for system (5.13), Hopf bifurcation is supercritical when a < 0; when a > 0, Hopf bifurcation is subcritical.

5.4. Derivation of the Saddle-node bifurcation condition of the model. The existence condition of saddle-nod bifurcation can be known from Lemma III [7].

Theorem 5.3. For system (5.13), let q^* be a variable parameter, and the derivative operator matrix at the equilibrium point is shown in (5.22). When, $q_0^* = -\varrho_0^2 V_e(\varrho_0)$, there exists $\beta = \begin{pmatrix} 1 \\ 0 \end{pmatrix}$ satisfying $L\beta = 0$.

Therefore,

(5.52)
$$\alpha L = 0 \Rightarrow \alpha = \left(\frac{2}{(\lambda + N)\Delta^2} \left((\lambda + N)\Delta - \frac{q_0^*}{\varrho_0}\right), 1\right).$$

It follows from Lemma III that

$$a = \partial \cdot \frac{\partial}{\partial q^*} f(x, q^*) \Big|_{(x_0, q_0^*)} = \left(\frac{2}{(\lambda + N)\Delta^2} \Big((\lambda + N)\Delta - \frac{q_0^*}{\varrho_0} \Big), 1 \right) \left(-\frac{0}{2\varrho_0} \frac{2}{T(\lambda + N)\Delta^2 q_0^*} \right)$$

$$= -\frac{2\varrho_0}{T(\lambda + N)\Delta^2 q_0^*} \neq 0,$$

$$b = \alpha \cdot \sum_{i=1}^n e_i \Big[\beta^T \frac{\partial^2}{\partial x^2} f(x, \lambda) \Big|_{(x_0, \lambda_0)} \beta \Big] = \left(\frac{2}{(\lambda + N)\Delta^2} \Big((\lambda + N)\Delta - \frac{q_0^*}{\varrho_0} \Big), 1 \right)$$

$$\cdot \left((1 \quad 0) \begin{pmatrix} 0 & 0 \\ 0 & 0 \end{pmatrix} \begin{pmatrix} 1 \\ 0 \end{pmatrix} \\ (1 \quad 0) \begin{pmatrix} 4V_e(\varrho_0) + 8\varrho_0 V_e'(\varrho_0) + 2\varrho_0^2 V_e''(\varrho_0) - 4c \\ T(\lambda + N)\Delta^2 q_0^* \\ -\frac{2q_0^*}{(\lambda + N)\Delta^2 \varrho_0^2} \\ T(\lambda + N)\Delta^2 q_0^* \end{pmatrix} - \frac{2q_0^*}{(\lambda + N)\Delta^2 \varrho_0^2} \Big]$$

$$= \frac{4V_e(\varrho_0) + 8\varrho_0 V_e'(\varrho_0) + 2\varrho_0^2 V_e''(\varrho_0) - 4c}{T(\lambda + N)\Delta^2 q_0^*} \neq 0.$$

Therefore, when $q_0^* = -\varrho_0^2 V_e'(\varrho_0)$, system (5.13) has a saddle-junction type bifurcation at $q^* = q_0^*$.

6. Numerical simulation

6.1. Simulation of the stop-and-go phenomenon. By simulating the traffic flow at different initial densities, it is possible to simulate the side walk stopping phenomenon of the traffic flow. In the uniform traffic flow, a small local disturbance is added, and the side walk stopping phenomenon can be clearly expressed in the small disturbance amplification phenomenon.

For the traffic flow model, considering the case of adding a small local perturbation to the initial uniform traffic flow, the expression for the initial density is given as follows

(6.1)
$$\varrho(x,0) = \varrho_0 + \Delta \varrho_0 \left\{ \cosh^{-2} \left[\frac{160}{L} \left(x - \frac{5L}{16} \right) \right] - \frac{1}{4} \cosh^{-2} \left[\frac{40}{L} \left(x - \frac{11L}{32} \right) \right] \right\}, \quad x \in [0, L],$$
(6.2)
$$v(x,0) = V(\varrho(x,0)), \quad x \in [0, L].$$

Where ϱ_0 is the initial density, $\Delta \varrho_0 = 0.01 \, \text{veh/m}$ is the perturbed density, $L = 32.2 \, \text{km}$ is the road section length, and the dynamic critical condition is given as follows

(6.3)
$$\varrho(1,t) = \varrho(2,t), \quad \varrho(L,t) = \varrho(L-1,t), \quad v(1,t) = v(2,t), \quad v(L,t) = v(L-1,t).$$

In order to facilitate the implementation of the simulation, the spatial spacing is taken to be equidistant and the time interval is taken to be 1S. The other parameters in the model are taken as follows (6.4)

$$T = 10 \text{ s}, V_f = 30 \text{ m/s}, \varrho_m = 0.2 \text{ veh/m}, r_0 = 126 \text{ m}, r = 250 \text{ m}, \varphi = 4, i = 0.15.$$

When the parameters are taken as above, the critical densities of the model are 0.045 veh/m and 0.070 veh/m, i.e., the traffic flow is linearly unstable when the initial density is ϱ_0 in the range of 0.045 veh/m to 0.070 veh/m.

Figure 2 explores the spatial and temporal evolution of the model for different initial densities of the density wave. As shown in Figure 2 (a), when the initial density is 0.041 veh/m, the density is within the stable range of the model, and when the small perturbation applied for it disappears with time, the density will return to a stable state, and the traffic flow will also reach a stable state at that time. In Figure 2 (b), the initial density of 0.045 veh/m is selected, which is within the unstable range of the model, and the magnitude of density fluctuation increases significantly at this time, and it evolves into the phenomenon of local clustering, indicating the phenomenon of traffic congestion, and the traffic system is in an unstable state at this time.

As shown in Figure 2 (b)–(e), when the initial density is between 0.045 veh/m and 0.070 veh/m, the density fluctuates widely and the traffic flow is in an unstable state, and the higher the initial density chosen for the traffic simulation, the larger the unstable region is. In addition, the traffic flow can evolve into local clusters, leading to the stop-and-go phenomenon. As shown in Figure 2 (f), the density wave returns to the steady state when the density increases to 0.075 veh/m, at which time the traffic flow gradually converges to a uniform flow. In summary, the unstable area of traffic flow ranges from 0.045 veh/m to 0.075 veh/m.

6.2. Influence of curve radius on traffic flow. In order to investigate the influence of curves on traffic flow, the traffic flow of different radii of curvature is simulated and verified, and other parameters are kept constant to illustrate the influence of curves on traffic flow through comparative analysis. Assuming that the vehicle travels at $40 \,\mathrm{km/h}$ on a curved section of road, the minimum safety radius of the vehicle at that velocity can be calculated as $r_0 = 126 \,\mathrm{m}$ from $r_0 = v^2/(127 \mu)$.

The larger the radius of curvature, the less curved the curve is. In real life, the more gentle the curve, the more stable the traffic condition is. From the density-time diagram, we can see that as the radius of curvature increases, the density wave is gradually dissipating and the unstable area of traffic flow is gradually decreasing, which also indicates that when the curve is gentler, the traffic condition is more stable. This is also consistent with the actual situation.

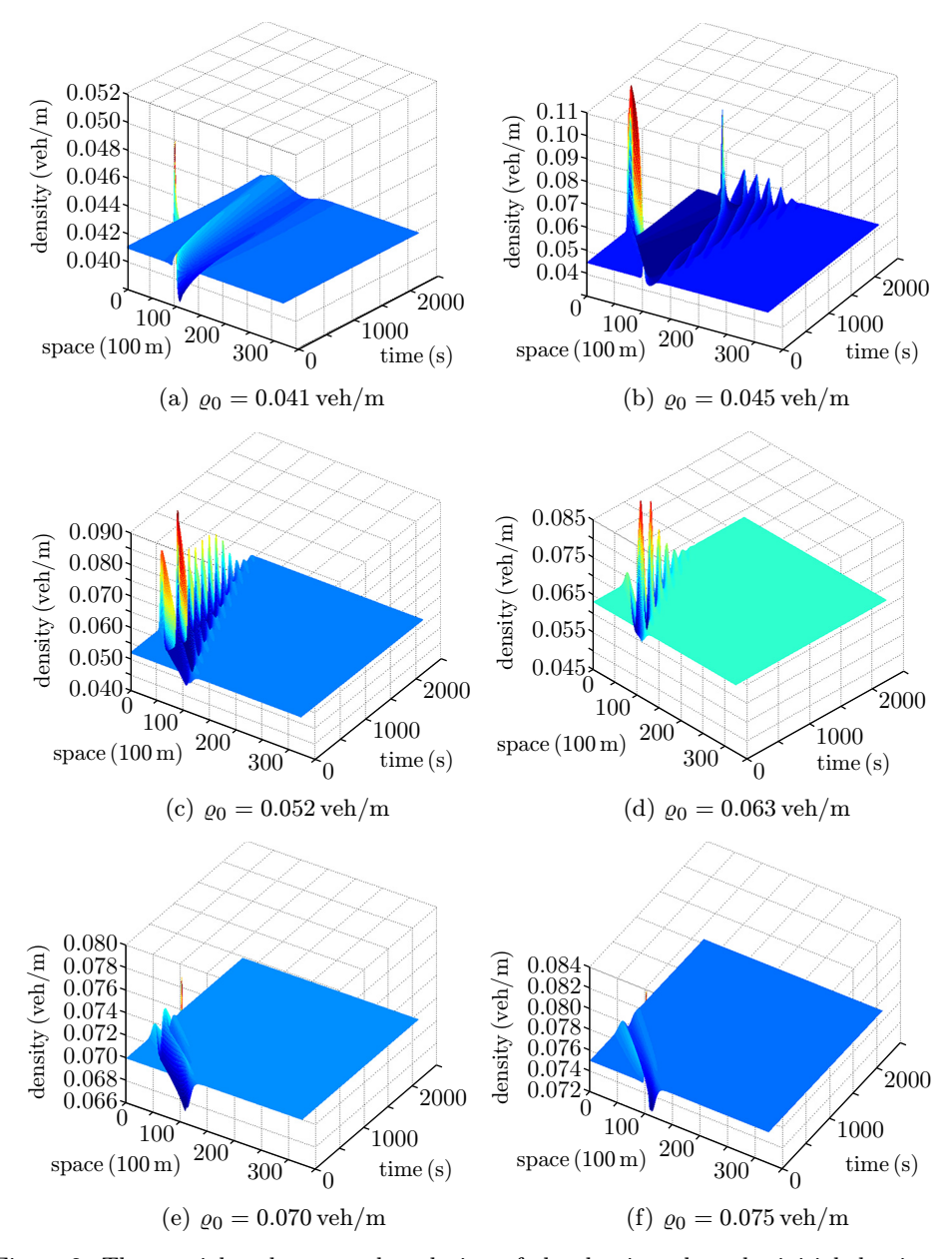


Figure 2. The spatial and temporal evolution of the density when the initial density ϱ_0 takes different values.

As shown in Figure 3 (c)–(d), in the curve radius of curvature larger gentle bend, the vehicle is basically in the state of free driving, the interaction between vehicles is smaller when the vehicle driving through the curve can still maintain the free state.

So, this case of the vehicle density change is smaller, density fluctuations are also smaller, the density to restore the steady state of the time used is also shorter, and soon the flow of traffic will reach the maximum, then the traffic flow will tend to the steady state, and the traffic density will also be stable.

Figure 3 (a)–(b) in the obvious density fluctuation area indicates the vehicle blockage area, that is, the local blockage phenomenon; density stabilization area indicates the smooth flow of vehicles, that is, vehicles running freely.

It can be seen from the density-time diagram that the traffic density fluctuates with the frequent stop-and-go behavior of vehicles, and this phenomenon leads to the local blockage phenomenon on the lane. The smaller the radius of curvature, the greater the magnitude and range of density fluctuations, which also indicates that the smaller the radius of curvature, the more obvious its effect on the traffic "bottleneck".

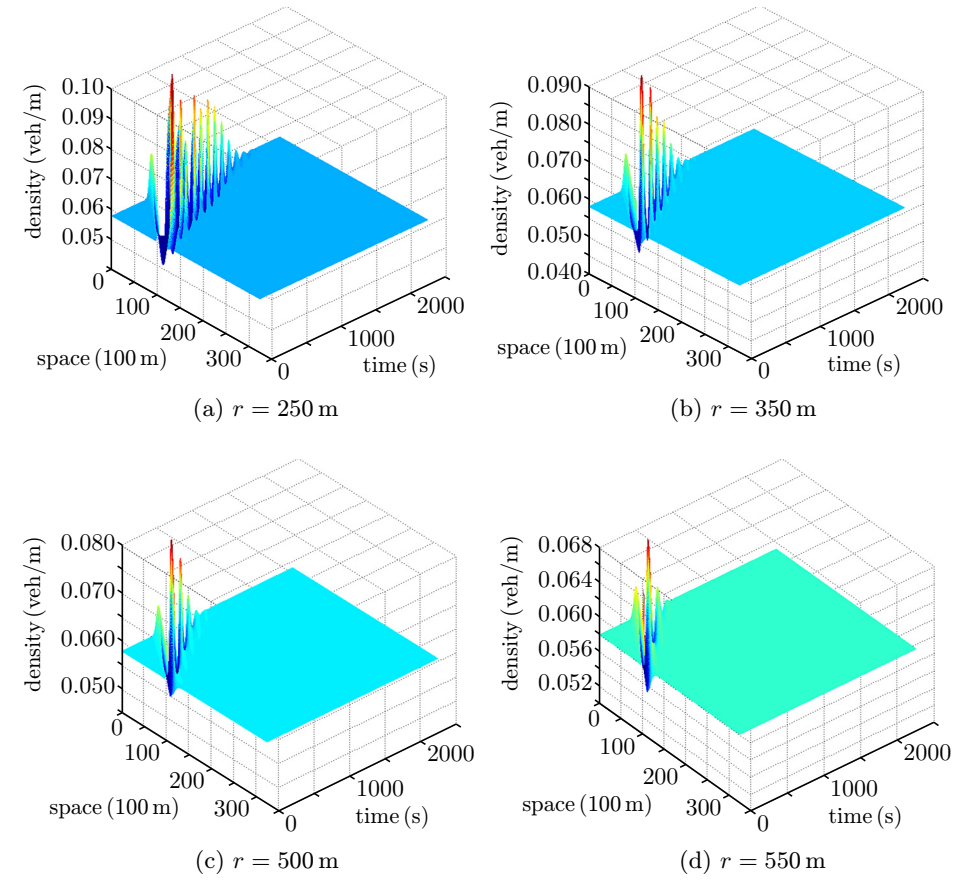


Figure 3. The spatial and temporal evolution of the density at different radii of curvature at initial density $\varrho_0 = 0.58 \text{ veh/m}$.

6.3. Influence of slope on traffic flow. Next, the effect of slope on traffic flow is considered, and the evolution of density spatial and temporal maps at different slopes is used to verify whether the theoretical results of the model are consistent with the actual traffic conditions.

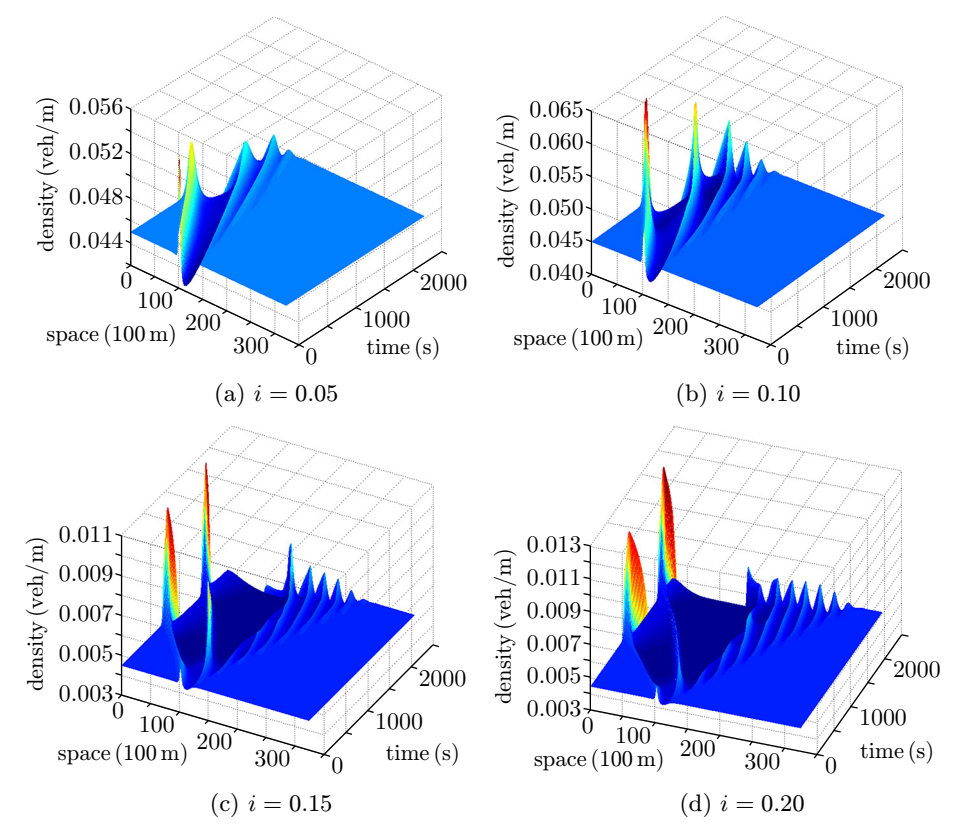


Figure 4. The spatial and temporal evolution of density at different slopes at initial density $\varrho_0 = 0.45 \text{ veh/m}.$

From Figure 4, it can be seen that with the increase of the slope, the amplitude and range of the density wave gradually increase, which indicates that when the vehicle is driving on a steeper section, the velocity change of the vehicle will be more obvious, and the driver's response to the stimulus (acceleration) is obviously stronger than that of driving on a flat road, and the traffic condition will become unstable. And as the slope increases, the unstable area of traffic flow also increases gradually. This also verifies the consistency of the theoretical analysis with the actual situation.

The simulation graph shows that the greater the slope of the ramp, the greater its effect on the driving. The driving velocity of the vehicle will drop significantly when it first drives into the ramp, and then the velocity change slowly stabilizes and finally reaches a uniform velocity. From the density spatial and temporal Figure 4(a)–(d) can be seen, in a certain period of time, that the vehicle density produced a sharp fluctuation, after that, the density fluctuation gradually calmed down, until finally reached a stable state. This is due to the fact that when the vehicle first enters the ramp, the driver's reaction is more intense and the velocity change is more obvious, at which time the traffic condition becomes unstable and may cause the phenomenon of traffic congestion. After that, when the driver decelerates to a stable state, the vehicle density will also tend to a stable state, which indicates that the traffic congestion phenomenon is gradually relieved. And the simulation graph shows that the larger the vertical slope is, the more significant is the effect on the traffic.

6.4. Analysis of bifurcation phenomenon in traffic flow. Through theoretical analysis and simulation, it is verified that the model is in line with the actual situation. The phenomena discussed above, such as traffic congestion and vehicles stop-and-go, occur frequently in actual traffic systems, but the mechanism that triggers these changes is difficult to be identified. Theoretically, the essence of the stability change of the traffic flow system is a bifurcation behavior, that is, when the parameters in the traffic system change and pass certain critical values, the qualitative state of the system will change suddenly. Bifurcation theory provides a new approach to reveal the inner regularity implied behind the nonlinear traffic flow phenomenon, so that traffic congestion can be detected and relieved in time. Therefore, the study of traffic flow bifurcation theory can not only effectively explain various traffic flow phenomena, but also contribute to the development of traffic planning and control. Next, we analyze the model using bifurcation theory.

By selecting different parameter values, system (5.13) can obtain different equilibrium points. Taking the equilibrium point $(\varrho_1, 0) = (0.0065, 0)$ as an example, various system bifurcations can be obtained by selecting different parameters as continuous variable parameters with the help of the bifurcation software package MATCONT.

When the initial value of the parameter q^* is set to 0.2, the actual calculation range of q^* is taken to be about -30 to 30, and two special points are found in this calculation range, which are a Hopf(H) bifurcation and a limit point (LP), as shown in Figure 5.

When the value of q^* is 0.832879, the state variable of the Hopf bifurcation obtained is 0.048993, indicating that the density of the vehicle at this time is $\varrho_0 = 0.048993 \text{ veh/m}$ and the two eigenvalues are (3.2711e-06) + 0.009684i and (3.2711e-06) - 0.009684i. The real part of this pair of conjugate eigenvalues is considered to be 0, which is an important condition to determine its Hopf bifurcation, and the maximum Lyapunov exponent is 9.269633e. Substituting the value of ϱ_0 into

the equation $-\varrho_0^2 V' e(\varrho_0)$, we get $-\varrho_0^2 V' e(\varrho_0) = 1.30756$. Obviously, the inequality 1.30756 > 0.832879 > 0 satisfies the derivation of the Hopf bifurcation condition of the model.

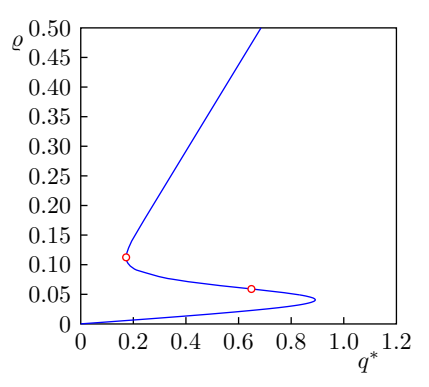


Figure 5. The bifurcation diagram for ϱ and q^* with appropriate parameters.

When the value of q^* is 0.172588, the limit point state variable is 0.112377, indicating that at this time the density of the vehicle is $\varrho_0=0.112377$ veh/m and the two eigenvalues are 2.1231e-05 and -0.018227. The latter eigenvalue is considered here to be 0, which is a sign that it is a limit point bifurcation. The other eigenvalue has a negative real part, which means it is a stable limit point (saddle knot bifurcation point). In addition, its quadratic normality coefficient is a=-2.089350e-01. Substituting the value of ϱ_0 into equation $-\varrho_0^2 V'e(\varrho_0)$, we get $-\varrho_0^2 V'e(\varrho_0)=0.172588$. Obviously, the equation $q_0^*=-\varrho_0^2 V'e(\varrho_0)$ satisfies the derivation of the saddle junction bifurcation condition of the model, and also verifies the consistency of the theoretical analysis with the numerical results.

Next, the stability of the traffic system is analyzed when the parameters are taken to some of the bifurcation thresholds calculated above. Firstly, the traffic flow near the Hopf bifurcation point is investigated, and the effect of the Hopf bifurcation on the traffic flow is illustrated by observing the change in the stability of the phase plane diagram of the system as the parameter q^* passes through 0.832879.

Figure 6 shows that there are two equilibrium points (0.02443,0) and (0.0554,0) when $q^* = 0.832879$. It can be seen from the figure that one spiral track line starts from the point (0.05,0) as time converges to the point (0.0554,0) as $z \to \infty$ and eventually evolves into an equal amplitude oscillation as $z \to -\infty$. The other spiral rail line tends to the outside of the above equal amplitude oscillation region as $z \to -\infty$, and tends to infinity as $z \to \infty$. So, there is a periodic solution between the two trajectories, so that no new equilibrium point appears at the Hopf bifurcation point, but a periodic solution is generated. This also verifies the consistency of the numerical results with the theoretical analysis. When $q^* = 0.832879$, a limit cycle

(LPC) appears and the first Yapunov exponent $a=9.269633\mathrm{e}$ is greater than zero, so this Hopf is in a subcritical state and this limit cycle is unstable. We can see from the spatial and temporal evolution of the density of the traffic flow that the uniform traffic flow becomes unstable and oscillates when it passes through the Hopf bifurcation point, which shows that the Hopf bifurcation has an impact on the traffic flow.

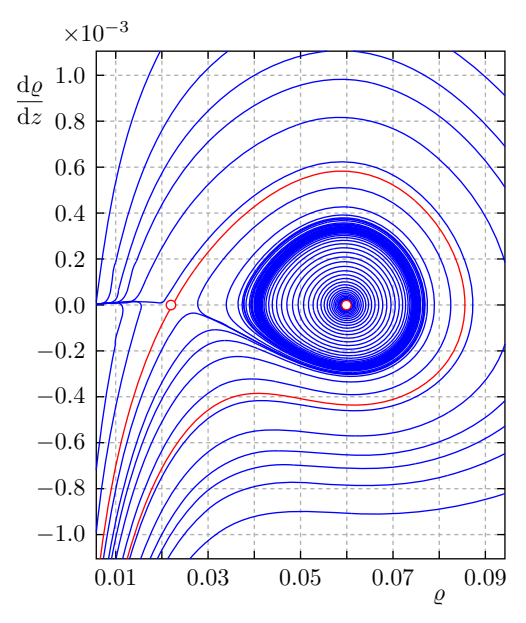


Figure 6. Phase plane diagram of Hopf bifurcation at parameter $q^* = 0.8328$.

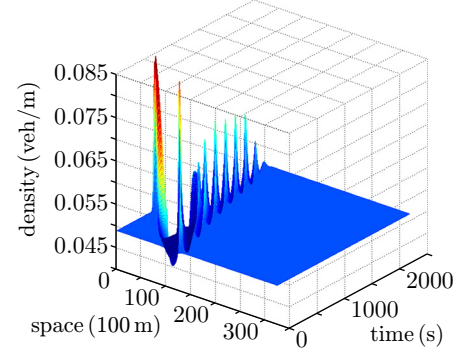


Figure 7. The spatial and temporal evolution of density when the initial density ϱ_0 takes the value of the Hopf bifurcation point.

When the initial density value is the Hopf bifurcation point corresponding to the state variable $\varrho_0 = 0.48993 \text{ veh/m}$, a small local perturbation of amplitude $\Delta \varrho_0 = 0.01 \text{ veh/m}$ is applied, and the same numerical simulation conditions as above are chosen, resulting in the density-time diagram of the system shown in Figure 7.

The complex phenomenon in congested traffic flow can be easily explained by the evolution of the density-time diagram with time. The effect of Hopf bifurcation on traffic flow can be clearly reflected by choosing the state variable of Hopf bifurcation point ($\varrho_0 = 0.48993 \, \text{veh/m}$) as the initial density of the density-time diagram. From the nature of Hopf bifurcation, it can be obtained that the system generates a periodic solution from the equilibrium point when the parameter passes through the bifurcation point. Since the initial density value at this point is in the unstable range of the model, the small perturbation on the initial uniform density is amplified, as shown in Figure 7, and then evolves into a dense go-go-stop wave of uniform amplitude, and then evolves into a larger, denser go-go-stop wave, which is consistent with the characteristics of the limit-loop solution. It illustrates that under the initial uniform traffic, the small perturbation changes to a walk-stop wave when the parameter is taken as the Hopf bifurcation point state variable, and also shows that the obtained conclusion is consistent with the actual phenomenon as well as the numerical calculation results, which also verify the correctness of the theoretical analysis.

In the following, we study the effect of the limit ring bifurcation on the traffic flow when the parameter q^* passes through 0.172588. When $q^* > 0.172588$, let $q^* = 0.18$, at this time the system has two equilibrium points (0.10165,0) and (0.12664,0), which are the focal point and the saddle point, as shown in Figure 8 (a). At this time, the traffic flow is stable in the region to the left of the red line in the figure, and unstable in the region to the right of the red line.

As the parameter q^* decreases, the red line moves to the left, and when the parameter q^* passes through $q^* = 0.172588$, a saddle-junction bifurcation occurs, as shown in Figure 8 (b). At this point, the two previous equilibrium points of the system merge into one equilibrium point (0.11522,0) now, and the system has only one zero eigenvalue. When the parameter q^* continues to decrease and is less than 0.172588, taking the value of $q^* = 0.16$, the equilibrium points all disappear and all the solutions move to the right, as shown in Figure 8 (c), and the traffic flow system becomes unstable.

7. Conclusions

In this paper, a macroscopic traffic flow model is improved with the FVD model as the theoretical basis, and a theoretical analysis and numerical simulation of the model are carried out by combining the mechanical properties of curves and ramps as well as the random disturbance factors such as weather environment. In the linear and nonlinear stability analysis, the neutral stability condition of the model and the KdV-Burgers equation are derived. The bifurcation analysis of the model is also carried out, and the conditions of existence and stability of a Hopf bifurcation and a saddle-

knot bifurcation are analyzed theoretically, and the bifurcation phenomena in the nonlinear traffic system are explained by the verification of simulation diagrams. The main conclusions are obtained as follows.

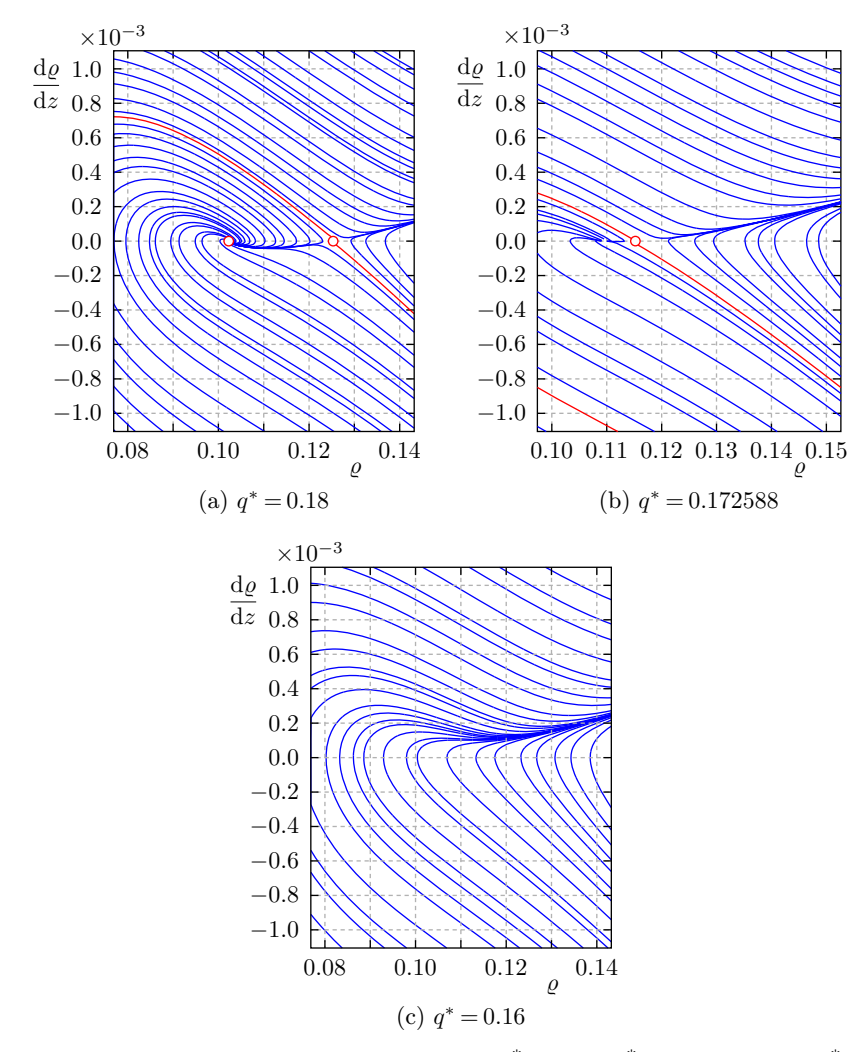


Figure 8. Phase plan of saddle-node bifurcation at $q^* = 0.18$, $q^* = 0.172588$ and $q^* = 0.16$.

Under the same condition of initial density of curved traffic, when vehicles pass through different curves at a certain speed, the smaller the radius of curvature, the more unstable the traffic flow system is, indicating that the smaller the radius of curvature of curves, the more obvious its influence on traffic flow.

The greater the slope of the ramp, the more unstable the traffic flow, which indicates that the greater longitudinal slope has a more significant effect on the traffic.

The bifurcation analysis of the model reveals that the stability of the system changes abruptly when the values of the parameters of the system change and span the values of the Hopf bifurcation point and the saddle-node bifurcation point. This is due to the changes in the qualitative states of the system, which are consistent with the changes between various traffic phenomena in real traffic, such as the transitions between the vehicle free-running state, the vehicle stop-and-go state, and the traffic congestion state, etc. The essence of the transitions between these different states is a bifurcation behavior. Therefore, the study of bifurcation behavior in traffic flow can well explain various nonlinear phenomena in real traffic and provide an effective theoretical basis for guiding and developing the planning and control management of traffic systems, so as to achieve the purpose of fundamentally alleviating and preventing traffic congestion.

A c k n o w l e d g m e n t s. The authors would like to thank the anonymous referees and the editor for their valuable opinions.

References

[1]	WH. Ai, ZK. Shi, DW. Liu: Bifurcation analysis of a speed gradient continuum traf-	
	fic flow model. Physica A 437 (2015), 418–429.	zbl MR do
[2]	M. Bando, K. Hasebe, A. Nakayama, A. Shibata, Y. Sugiyama: Dynamical model of traf-	
	fic congestion and numerical simulation. Phys. Rev. E (3) 51 (1995), 1035–1042.	doi
[3]	J. F. Cao, C. Z. Han, Y. W. Fang: Nonlinear Systems Theory and Application. Xi'an Jiao	
	Tong University Press, Xi'an, 2006; ISBN 7-5605-2140-1. (In Chinese.)	
[4]	F. A. Carrillo, J. Delgado, P. Saavedra, R. M. Velasco, F. Verduzco: Traveling waves,	
	catastrophes and bifurcations in a generic second order traffic flow model. Int. J. Bifur-	
	cation Chaos Appl. Sci. Eng. 23 (2013), Article ID 1350191, 15 pages.	zbl MR do
[5]	B. Chen, D. Sun, J. Zhou, W. Wong, Z. Ding: A future intelligent traffic system with	
	mixed autonomous vehicles and human-driven vehicles. Inform. Sci. 529 (2020), 59-72.	MR doi
[6]	N. Cui, B. Chen, K. Zhang, Y. Zhang, X. Liu, J. Zhou: Effects of route guidance strate-	
	gies on traffic emissions in intelligent transportation systems. Physica A 513 (2019),	
	32–44.	doi
[7]	C. F. Daganzo, J. A. Laval: Moving bottlenecks: A numerical method that converges in	
	flows. Transp. Res., Part B 39 (2005), 855–863.	doi
[8]	J. Delgado, P. Saavedra: Global bifurcation diagram for the Kerner-Konhäuser traffic	
	flow model. Int. J. Bifurcation Chaos Appl. Sci. Eng. 25 (2015), Article ID 1550064, 18	
	pages.	zbl MR do
[9]	A. K. Gupta, I. Dhiman: Phase diagram of a continuum traffic flow model with a static	
	bottleneck. Nonlinear Dyn. 79 (2015), 663–671.	MR doi
10]	A. K. Gupta, V. K. Katiyar: Analyses of shock waves and jams in traffic flow. J. Phys.	
	A, Math. Gen. 38 (2005), 4069–4083.	zbl MR do
11]	A. K. Gupta, V. K. Katiyar: A new anisotropic continuum model for traffic flow. Physica	
-	A 368 (2006), 551–559.	doi
12]	A. K. Gupta, V. K. Katiyar: Phase transition of traffic states with on-ramp. Physica A	
	<i>371</i> (2006), 674–682.	doi

[13]	A. K. Gupta,	P. Redhu:	Jamming	transition	of a t	wo-dim	ensiona	al traffi	c dynamics	with	
	consideration	of optima	al current	difference.	Phys.	Lett.,	A 377 ((2013),	2027 - 2033.		zbl

- [14] A. K. Gupta, S. Sharma: Nonlinear analysis of traffic jams in an anisotropic continuum model. Chin. Phys. B 19 (2010), Article ID 110503, 9 pages.
- [15] A. K. Gupta, S. Sharma: Analysis of the wave properties of a new two-lane continuum model with the coupling effect. Chin. Phys. B 21 (2012), Article ID 015201, 15 pages.
- [16] Y. Igarashi, K. Itoh, K. Nakanishi, K. Ogura, K. Yokokawa: Quasi-solitons in dissipative systems and exactly solvable lattice models. Phys. Rev. Lett. 83 (1999), 718–721.
- [17] Y. Igarashi, K. Itoh, K. Nakanishi, K. Ogura, K. Yokokawa: Bifurcation phenomena in the optimal velocity model for traffic flow. Phys. Rev. E (3) 64 (2001), Article ID 047102.
- [18] R. Jiang, Q. Wu, Z. Zhu: Full velocity difference model for a car-following theory. Phys. Rev. E (3) 64 (2001), Article ID 017101.
- [19] R. Jiang, Q.-S. Wu, Z.-J. Zhu: A new continuum model for traffic flow and numerical tests. Transp. Res., Part B 36 (2002), 405–419.
- [20] B. S. Kerner, P. Konhäuser: Cluster effect in initially homogeneous traffic flow. Phys. Rev. E (3) 48 (1993), 2335–2338.
- [21] Y. A. Kuznetsov: Bifurcations of equilibria and periodic orbits in n-dimensional dynamical systems. Elements of Applied Bifurcation Theory. Applied Mathematical Sciences 112. Springer, New York, 1998, pp. 151–194.
- [22] L. Lei, Z. Wang, Y. Wu: Modeling and analyzing for a novel continuum model considering self-stabilizing control on curved road with slope. CMES, Comput. Model. Eng. Sci. 131 (2022), 1815–1830.
- [23] D. Ling, X. P. Jian: Stability and bifurcation characteristics of a class of nonlinear vehicle following model. J. Traffic and Transportation Engineering and Information 7 (2009), 6–11.
- [24] G. Ma, M. Ma, S. Liang, Y. Wang, H. Guo: Nonlinear analysis of the car-following model considering headway changes with memory and backward looking effect. Physica A 562 (2021), Article ID 125303, 12 pages.
- [25] G. Ma, M. Ma, S. Liang, Y. Wang, Y. Zhang: An improved car-following model accounting for the time-delayed velocity difference and backward looking effect. Commun. Nonlinear Sci. Numer. Simul. 85 (2020), Article ID 105221, 10 pages.
- [26] X. P. Meng, L. Y. Yan: Stability analysis in a curved road traffic flow model based on control theory. Asian J. Control 19 (2017), 1844–1853.
- [27] G. Orosz, R. E. Wilson, B. Krauskopf: Global bifurcation investigation of an optimal velocity traffic model with driver reaction time. Phys. Rev. E (3) 70 (2004), Article ID 026207, 10 pages.
- [28] P. Redhu, A. K. Gupta: Delayed-feedback control in a Lattice hydrodynamic model. Commun. Nonlinear Sci. Numer. Simul. 27 (2015), 263–270.
- [29] J. Zeng, Y. Qian, D. Xu, Z. Jia, Z. Huang: Impact of road bends on traffic flow in a single-lane traffic system. Math. Probl. Eng. 2014 (2014), Article ID 218465, 6 pages. Zbl MR doi
- [30] C. Zhai, W. Wu: A new car-following model considering driver's characteristics and traffic jerk. Nonlinear Dyn. 93 (2018), 2185–2199.
- [31] C. Zhai, W. Wu: Car-following model based delay feedback control method with the gyroidal road. Int. J. Mod. Phys. C 30 (2019), Article ID 1950073, 14 pages.
- [32] C. Zhai, W. Wu: Lattice hydrodynamic model-based feedback control method with traffic interruption probability. Mod. Phys. Lett. B 33 (2019), Article ID 1950273, 16 pages. MR doi
- [33] C. Zhai, W. Wu: A modified two-dimensional triangular lattice model under honk environment. Int. J. Mod. Phys. C 31 (2020), Article ID 2050089, 16 pages.

doi

MR doi

MR doi

MR doi

doi

zbl MR doi

zbl MR doi

zbl MR doi

zbl MR doi

doi

- [34] C. Zhai, W. Wu: Lattice hydrodynamic modeling with continuous self-delayed traffic flux integral and vehicle overtaking effect. Mod. Phys. Lett. B 34 (2020), Article ID 2050071, 15 pages.
- 2050071, 15 pages.

 [35] C. Zhai, W. Wu: A macro traffic flow model with headway variation tendency and bounded rationality. Mod. Phys. Lett. B 35 (2021), Article ID 2150054, 15 pages.

 MR doi

zbl MR doi

MR doi

- [36] C. Zhai, W. Wu: Designing continuous delay feedback control for lattice hydrodynamic model under cyber-attacks and connected vehicle environment. Commun. Nonlinear Sci. Numer. Simul. 95 (2021), Article ID 105667, 18 pages.
- [37] P. Zhang, Y. Xue, Y.-C. Zhang, X. Wang, B.-L. Cen: A macroscopic traffic flow model considering the velocity difference between adjacent vehicles on uphill and downhill slopes. Mod. Phys. Lett. B 34 (2020), Article ID 2050217, 18 pages.

Authors' addresses: Wenhuan Ai (corresponding author), Ting Zhang, College of Computer Science and Engineering, Northwest Normal University, 967 Anning East Rd, Lanzhou, Gansu, 730070, P. R. China, e-mail: wenhuan618@163.com, 2624667019@qq.com; Dawei Liu, College of Electrical Engineering, Lanzhou Institute of Technology, 1 Gongjiaping E Road, Lanzhou, Gansu, 730050, P. R. China, e-mail: liudawei20120901@163.com.